






Cite this: *CrystEngComm*, 2020, 22, 821

The incorporation of heterovalent copper-oxo and copper-halide clusters for the fabrication of three porous cluster organic frameworks: syntheses, structures and iodine adsorption/release study†

Jin-Hua Liu,^a Jing Zhang,^a Dan Zhao,^b Li-Dan Lin,^a Yan-Qiong Sun,^a ^a
 Xin-Xiong Li ^{*a} and Shou-Tian Zheng ^{*a}

Three porous heterovalent cluster organic frameworks $\text{Cu}_2(\text{H}_2\text{O})(\text{Cu}_4\text{I}_4)(\text{INA})_4\cdot\text{solvent}$ (**1**), $\text{Cu}_2(\text{H}_2\text{O})_2(\text{Cu}_4\text{I}_4)_2(\text{INA})_4(\text{DABCO})_2\cdot 2\text{DMA}$ (**2**) and $[(\text{Cu}_2)_2(\text{PVBA})_8(\text{Cu}_4\text{I}_4)]\cdot\text{DMF}$ (**3**) (HINA = isonicotinic acid, DABCO = 1,4-diazabicyclo[2.2.2]octane, HPVBA = 4-(2-(4-pyridyl)ethenyl) benzoic acid, DMF = *N,N'*-dimethylformamide, DMA = *N,N'*-dimethylacetamide) have been solvothermally synthesized and structurally characterized. Crystal structure analyses indicate that compounds **1** and **2** are constructed from planar four-connected $\text{Cu}_2(\text{CO}_2)_4$ secondary building units (SBUs) and tetrahedral four-connected Cu_4I_4 SBUs, while compound **3** is composed of octahedral six-connected $\text{Cu}_2(\text{CO}_2)_4$ SBUs and tetrahedral four-connected Cu_4I_4 SBUs. All these frameworks possess nano-sized 1-dimensional channels. Furthermore, the thermal and chemical stabilities, gas adsorption properties and iodine adsorption/release ability of compound **2** have been systematically studied.

Received 5th November 2019,
 Accepted 19th December 2019

DOI: 10.1039/c9ce01745c

rsc.li/crystengcomm

Introduction

Metal-organic frameworks (MOFs) are extensively researched on account of their structural novelties, high surface area and high porosity; they have various potential applications in photoluminescence, chemical sensing, catalysis and gas storage.^{1–3} However, the studies of heterovalent MOFs are still obviously lagging far behind because the metal ions of an element with different valences usually cannot easily coexist under the same synthetic conditions. Owing to the efforts from chemists across the world, some strategies have been designed to stabilize heterovalent metal ions in one reaction, and this area has started to advance recently. For instance, two iso-structural cluster-based MOFs constructed from heterovalent $\text{Ni}_2^{2+}\text{Ni}^{3+}$ and $\text{Co}_2^{2+}\text{Co}^{3+}$ trinuclear and Ni_6^{2+} and Co_6^{2+} hexanuclear clusters have been assembled.⁴ Besides, large nanosized Zn_{70} -cage MOFs built from heterovalent $[\text{Zn}^+_8]$ clusters and Zn^{2+} ions were also constructed.⁵ Furthermore, a heterovalent Ce-MOF consisting of Ce^{3+} and

Ce^{4+} ions and showing oxidase-like activity has been reported.⁶ Most interestingly, polyoxometalate (POM)-based MOFs constructed from nanometer scale heterovalent $\{\text{V}_{16}\}$ clusters were also reported.⁷

Compared to the above-mentioned Ni/Co/Zn/Ce/V-based heterovalent MOFs, Cu-based heterovalent MOFs are becoming a new hottest research topic due to the flexible coordination characteristics of copper ions.⁸ Generally speaking, Cu^{2+} can form various copper-oxo clusters easily, including square paddlewheel dimers $[\text{Cu}_2(\text{CO}_2)_4]$,^{9,10} trigonal $[\text{Cu}_3\text{O}]$ species,^{11,12} and tetra-nuclear rod-like $[\text{Cu}_4\text{O}_2]$ compounds.¹³ Cu^+ ions tend to create a variety of cuprous-halide clusters, such as rhomboid dimers Cu_2I_2 ,^{14–16} cubane tetramers Cu_4I_4 ,^{17–20} hexagonal prisms Cu_6I_6 (ref. 21 and 22) and rare Cu_8I_6 clusters.²³ So far, some representative examples based on heterovalent copper clusters have been reported, which demonstrate interesting abilities for the adsorption and desorption of guest molecules.^{24,32–35}

Iodine is one of the important trace elements needed by the human body, and it has been provoking great interest in the fields of environmental chemistry, bioscience and nuclear industries.²⁵ Lately, the research of iodine adsorption has attracted increasing attention. Currently, many materials have been used for iodine adsorption, such as activated carbons, porous silicas and organic polymers.²⁶ In particular, some MOFs also show preferable performance of iodine species adsorption in a high concentration iodine solution

^a State Key Laboratory of Photocatalysis on Energy and Environment, College of Chemistry, Fuzhou University, Fuzhou, Fujian 350108, China.

E-mail: lxx@fzu.edu.cn, stzheng@fzu.edu.cn

^b Fuqing Branch of Fujian Normal University, Fuzhou, Fujian 350002, China

† Electronic supplementary information (ESI) available: Synthetic details, structural figures, and spectrum data. CCDC 1910018–1910020. For ESI and crystallographic data in CIF or other electronic format see DOI: 10.1039/c9ce01745c

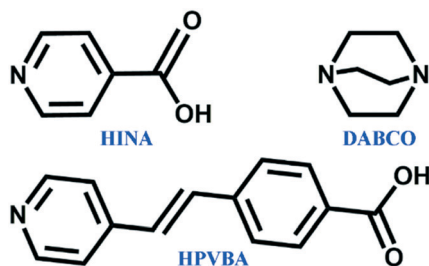
and vapor.^{27–31} For instance, ZIF-8 with sodalite cages can capture iodine molecules *via* bonding with the skeleton, exhibiting detailed structural evidence for capturing I₂.²⁷ The activated {[Zn₃(DL-lac)₂(pybz)₂]-2.5DMF}_n (Hpybz = 4-(pyridin-4-yl)benzoic acid) possesses rigid double walls and square-shaped channels, which can capture iodine molecules *via* the I₂ π-electrons of the surface of the walls.²⁸ HKUST-1 with three types of cavities and a high surface area displays preferential adsorption of iodine molecules over water *via* strong interactions between I₂ and the HKUST-1 skeleton.²⁹ Liu's group also reported a series of Cu-based heterovalent MOFs for iodine adsorption, which displayed high adsorption capacity.^{32–35} Inspired by these ideas, we are particularly interested in designing novel Cu-based heterovalent MOFs and further study their performance for iodine adsorption.

Herein, by introducing three different bridging ligands (Scheme 1), three novel Cu-based heterovalent MOFs [Cu₂(H₂O)₂(Cu₄I₄)(INA)₄]-solvent (**1**) (HINA = isonicotinic acid), [Cu₂(H₂O)₂(Cu₄I₄)(INA)₄(DABCO)₂]-2DMA (**2**) (DABCO = 1,4-diazabicyclo[2.2.2]octane, DMA = *N,N'*-dimethylacetamide) and [(Cu₂)₂(PVBA)₈(Cu₄I₄)]-DMF (**3**) (HPVBA = 4-(2-(4-pyridyl)ethenyl) benzoic acid, DMF = *N,N'*-dimethylformamide) were obtained; all these MOFs showed 3-dimensional (3D) neutral structures based on the paddle-wheel Cu₂(CO₂)₄ and Cu₄I₄ clusters. Interestingly, **1** displayed a large honeycomb-like 3D structure with 1D hexagonal channels with a size of 2.4 × 2.7 nm²; **2** displayed a very different 2-fold interpenetrated network and good thermal and solvent stabilities. Furthermore, **3** could be described as a neutral skeleton constructed from Cu₂(CO₂)₄ and PVBA[−] bridges, which encapsulated Cu₄I₄ in alternating channels. Also, **2** exhibited good capacity for the adsorption/release of iodine molecules in a solvent. Additionally, the gas sorption of **2** was investigated.

Experimental

Materials and measurements

All reactants and solvents were obtained from commercial sources and used for reactions without further purification. 4-(2-(4-Pyridyl)ethenyl) benzoic acid (HPVBA) was synthesized according to literature procedures.³⁶ Powder X-ray diffraction (PXRD) data were collected on a Rigaku DMAX 2500 diffractometer working with Cu-Kα radiation (λ = 1.54178 Å)



Scheme 1 Schematic structural illustration of ligands HINA, DABCO and HPVBA in this work.

over the 2θ range of 5–50° at room temperature. Thermogravimetric analyses (TGA) were executed on a Mettler Toledo TGA/SDTA 851e analyzer under a heating speed from 10 °C to 800 °C in air. Elemental analyses (EA) for C, H and N were carried out on a Vario MICRO elemental analyzer. UV-vis adsorption spectra were obtained by using a PerkinElmer Lambda 35 spectrophotometer to monitor the release procedure. The infrared (IR) spectra were measured on Nicolet iS50 at an ambient temperature.

Gas adsorption analysis

The surface area and pore distribution were tested by N₂ adsorption by an Accelerated Surface Area and Porosimetry 2020 (ASAP-2020) surface area instrument at 77 K. The CO₂ adsorption isotherms were tested at 273 and 298 K. The gases used during all measurements were 99.999% pure. Before measurements, the samples of **2** were immersed in fresh ethanol under room temperature for 5 days in order to exchange high-boiling-point guests. The activated samples of **2** were obtained by degassing the exchanged crystals under high vacuum at 333 K for 8 h.

Synthesis of Cu₂(H₂O)(Cu₄I₄)(INA)₄-solvent (**1**)

In a 20 mL quartz bottle, CuCl₂·2H₂O (0.23 mmol, 40 mg), CuI (0.63 mmol, 120 mg), HINA (0.32 mmol, 40 mg) and 4,4'-biphenyldicarboxylic acid (0.10 mmol, 26 mg) were mixed in DMA (2 mL) and *N,N'*-diethylformamide (DEF, 2 mL) and further stirred for 1 h. Then, the final mixture was sealed and kept at 100 °C in an oven for 4 days. After cooling to an ambient temperature, green block crystals of **1** suitable for single crystal X-ray diffraction measurements were harvested by filtration, washing with DMA and drying in air. Yield: *ca.* 14% (based on CuI). IR (KBr pellet, ν/cm^{−1}): 3358(w), 2940(w), 1598(w), 1557(m), 1501(s), 1381(w), 1265(s), 1179(s), 1052(m), 1013(m), 846(s), 770(m), 684(m), 588(m).

Synthesis of Cu₂(H₂O)₂(Cu₄I₄)₂(INA)₄(DABCO)₂-2DMA (**2**)

In a 20 mL quartz bottle, CuCl₂·2H₂O (0.23 mmol, 40 mg), CuI (0.42 mmol, 80 mg), HINA (0.32 mmol, 40 mg), and DABCO (0.18 mmol, 20 mg) were mixed in 5 mL DMA and stirred for 1 h. Then, the final mixture was sealed and kept at 100 °C for 4 days. After cooling to an ambient temperature, green square crystals of **2** suitable for single crystal X-ray diffraction measurements were harvested by filtration, washing with DMA and drying in air. Yield: *ca.* 52% (based on CuI): C, H, N elemental analysis (wt%) for **2**: calcd C 20.53, H 2.42, N 5.44; found: C 20.74, H 2.16, N 5.49. IR (KBr pellet, ν/cm^{−1}): 3414(w), 2940(m), 2885(s), 1608(w), 1547(s), 1497(m), 1391(w), 1265(m), 1179(m), 1052(s), 1013(w), 861(s), 796(s), 765(m), 680(m), 583(m).

Synthesis of [(Cu₂)₂(PVBA)₈(Cu₄I₄)]-DMF (**3**)

In a 20 mL quartz bottle, CuI (0.26 mmol, 50 mg), HPVBA (0.14 mmol, 30 mg) were mixed in 4 mL DMF and stirred for

1 h. Then, the final mixture was sealed and kept at 100 °C for 4 days. After cooling to an ambient temperature, pale green stick crystals of **3** suitable for single crystal X-ray diffraction measurements were obtained by filtration, washing with DMF and drying in air. Yield: ca. 18% (based on CuI). C, H, N elemental analysis (wt%) for **3**: calcd C 47.91, H 3.04, N 4.37; found: C 47.07, H 2.86, N 4.29. IR (KBr pellet, ν/cm^{-1}): 2920(m), 2082(m), 1663(w), 1593(w), 1537(m), 1492(m), 1370(w), 1245(s), 1209(s), 1088(m), 1013(m), 942(w), 831(w), 800(w), 760(w), 669(w), 538(w).

Single crystal structure analyses

Single crystal X-ray diffraction (SCXRD) data were collected on a Bruker Smart Apex II CCD diffractometer at 175 K using graphite monochromated Cu $K\alpha$ radiation ($\lambda = 1.54178 \text{ \AA}$) for **1** and **3** and 175 K using graphite monochromated Mo/ $K\alpha$ radiation ($\lambda = 0.71073 \text{ \AA}$) for **2**. The direct method was used to solve the structures of **1**–**3**. The final structures of **1**–**3** were refined through full-matrix least-squares refinements based on F^2 in SHELX-2014 package.³⁷ All hydrogen atoms attached to carbon atoms were geometrically placed and refined isotropically. All atoms except hydrogen atoms were refined anisotropically. The disordered solvent molecules in **1**–**3** were eliminated by the SQUEEZE³⁸ function in PLATON. Crystallographic data and structure refinements for **1**–**3** are summarized in Table 1. The supplementary crystallographic data for this

paper are deposited in CCDC database with the codes of 1910020 (**1**), 1910018 (**2**) and 1910019 (**3**).

Results and discussion

Structural description of **1**

SCXRD analysis revealed that **1** crystallized in the trigonal $R\bar{3}c$ space group. Its asymmetric unit consisted of two independent Cu^+ ions (Cu1, Cu2), one Cu^{2+} (Cu3) ion, two I^- ions, two fully deprotonated INA^- ligands and one terminally coordinated water molecule (Fig. S1†). As shown in Fig. 1a, Cu^{2+} exhibits square-pyramidal geometry by four equatorial oxygen atoms from four COO^- of INA^- ligands and one axial-position oxygen atom from a coordinated water molecule. Typically, two five-coordinated Cu^{2+} atoms generated a classical paddle-wheel $\text{Cu}_2(\text{CO}_2)_4$ cluster *via* INA^- bridging. Furthermore, each pyridyl of INA^- attached to a cubane-like Cu_4I_4 cluster (Fig. 1b). The Cu–I, Cu–O and Cu–N bond lengths were in the ranges of 2.63–2.79, 1.92–2.10, and 1.95–2.03 \AA , which were comparable with those reported in a previous work.³⁹ Generally, the $\text{Cu}_2(\text{CO}_2)_4$ cluster could be viewed as a square SBU, while the Cu_4I_4 cluster could be regarded as a tetrahedral SBU. The linkage of these two different 4-connected SBUs gave rise to a 3D framework structure (Fig. 1c). The most striking structural feature of this framework is that it possesses extra-large 1D hexagonal channels with the size of about $2.4 \times 2.7 \text{ nm}^2$ along the c axis (Fig. 1d and i). The basic unit of these channels is made up

Table 1 Crystal data and structure refinement for **1**–**3**

	1	2	3
Empirical formula	$\text{C}_{24}\text{H}_{20}\text{Cu}_6\text{I}_4\text{N}_4\text{O}_{10}$	$\text{C}_{36}\text{H}_{44}\text{Cu}_{10}\text{I}_8\text{N}_8\text{O}_{10}$	$\text{C}_{112}\text{H}_{80}\text{Cu}_8\text{I}_4\text{N}_8\text{O}_{16}$
Formula weight	1413.34	2399.39	2809.84
Crystal system	Trigonal	Orthorhombic	Monoclinic
Space group	$R\bar{3}c$	$Cmca$	$C2/c$
a (\AA)	49.26 (9)	29.00 (3)	63.59 (2)
b (\AA)	49.26 (9)	17.61 (15)	19.66 (7)
c (\AA)	35.34 (14)	16.93 (15)	41.56 (14)
V (\AA^3)	74 301 (4)	8654.1 (13)	39 490 (2)
Z	18	4	8
$F(000)$	11 842	5140	11 038
θ range/ $^\circ$	2.706 to 50.513	1.810 to 25.041	1.829 to 66.895
Limiting indices	$-49 \leq h \leq 46$ $-49 \leq k \leq 48$ $-33 \leq l \leq 33$	$-28 \leq h \leq 34$ $-16 \leq k \leq 20$ $-14 \leq l \leq 20$	$-72 \leq h \leq 75$ $-22 \leq k \leq 21$ $-49 \leq l \leq 38$
ρ_{calcd} (g cm^{-3})	0.569	2.110	0.945
Temperature (K)	175(2)	175(2)	175(2)
μ (mm^{-1})	6.820	5.295	6.137
Refl. collected	48 890	14 839	92 426
Independent refl.	8589	3879	32 917
Parameters	217	166	1333
R_{int}	0.0977	0.0239	0.0473
GOF on F^2	1.003	1.050	1.065
Final R indices ($I = 2\sigma(I)$)	$R_1 = 0.0684$, $wR_2 = 0.1879$	$R_1 = 0.0315$, $wR_2 = 0.0896$	$R_1 = 0.0894$, $wR_2 = 0.3184$
R indices (all data)	$R_1 = 0.1111$, $wR_2 = 0.2071$	$R_1 = 0.0384$, $wR_2 = 0.0926$	$R_1 = 0.0973$, $wR_2 = 0.3334$

$R_1 = \sum ||F_o| - |F_c|| / \sum |F_o|$. $wR_2 = [\sum w(F_o^2 - F_c^2)^2 / \sum w(F_o^2)^2]^{1/2}$; $w = 1/[\sigma^2(F_o^2) + (xP)^2 + yP]$, $P = (F_o^2 + 2F_c^2)/3$, where $x = 0.116100$, $y = 0$ for **1**; $x = 0.054600$, $y = 57.403599$ for **2**; $x = 0.280000$, $y = 0$ for **3**.

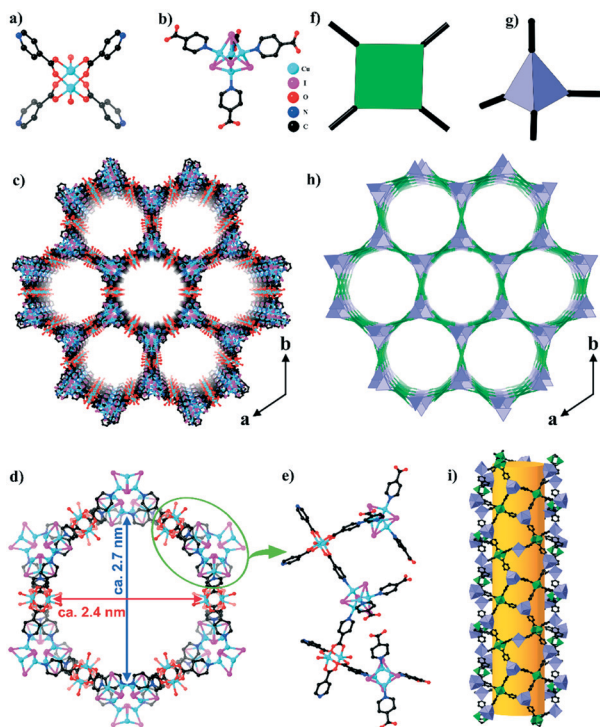


Fig. 1 Crystal structure of **1**: a and b) the paddle-wheel $\text{Cu}_2(\text{CO}_2)_4$ and cubane-like Cu_4I_4 clusters. c) View of the 3D honeycomb-like framework structure. d) View of the 1D hexagonal channel with the size of $2.4 \times 2.7 \text{ nm}^2$. e) The connection mode between $\text{Cu}_2(\text{CO}_2)_4$ and Cu_4I_4 clusters. f and g) The topological representation of $\text{Cu}_2(\text{CO}_2)_4$ and Cu_4I_4 clusters. h) The topological representation of 3D honeycomb-like framework. i) View of 1D hexagonal channels viewed along the b axis.

of twelve $\text{Cu}_2(\text{CO}_2)_4$ clusters, eighteen Cu_4I_4 clusters and forty-two INA^- ligands (Fig. 1e).

Recently, some 3D honeycomb-like framework structures have been reported.⁴⁰ However, examples based on two different cluster SBUs are very limited. As far as we know, **1** represents an important new member of honeycomb-like framework structures containing extra-large channels. From the topological point of view, the $\text{Cu}_2(\text{CO}_2)_4$ and Cu_4I_4 clusters can be considered as a 4-connected planar node and a 4-connected tetrahedral node, respectively (Fig. 1f and g). The whole framework can be simplified as 4,4-connected topology with the Schläfli symbol of $\{4^2 \cdot 6^2 \cdot 8^2\}\{4^2 \cdot 6^4\}$ (Fig. 1h). PLATON calculations indicate that the potential guest-accessible volume of the framework is 61758.7 \AA^3 , corresponding to 83.1% of the total crystal volume (74301.0 \AA^3).

Structural description of **2**

SCXRD analysis revealed that **2** crystallized in the orthorhombic $Cmca$ space group. As shown in Fig. S2† its asymmetric unit comprises two Cu^+ ions (Cu1, Cu2), half of a Cu^{2+} (Cu3) ion, two I^- ions, one INA^- ligand, half of a DABCO ligand and half of a terminal coordinated water molecule. The basic structural SBUs in **2** were the same as

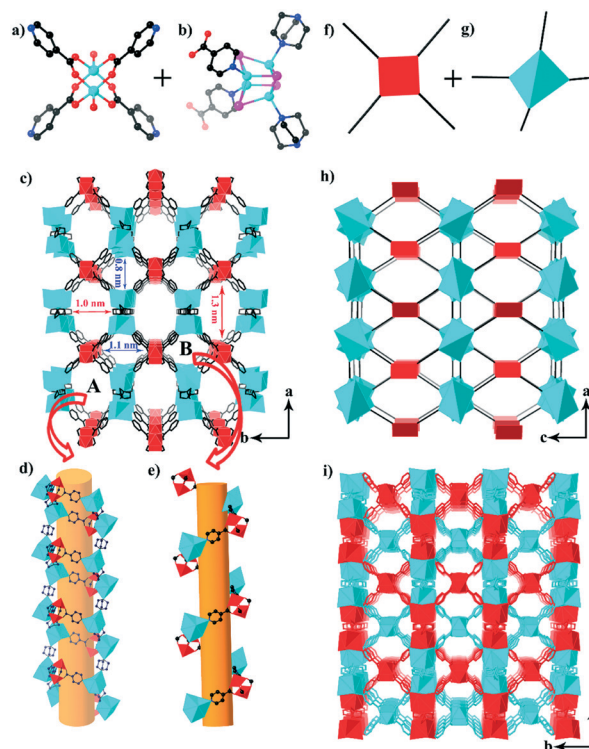


Fig. 2 Crystal structure of **2**: a and b) the paddle-wheel $\text{Cu}_2(\text{CO}_2)_4$ and cubane-like Cu_4I_4 clusters. c) View of the 3D framework along the c axis. d and e) View of tubular channels. f and g) The topological representation of $\text{Cu}_2(\text{CO}_2)_4$ and Cu_4I_4 clusters. h) The topology of the 3D framework. i) View of the 2-fold interpenetrated framework structure in **2**.

those in **1** (Fig. 2a and b). However, the final framework structure was much different from that of **1**. This was because an additional bridging ligand DABCO was involved in bridging Cu_4I_4 SBUs. As shown in Fig. 2b, Cu_4I_4 SBU is stabilized by two INA^- and two DABCO ligands, which is different from that in **1**. Interestingly, the framework of **2** contained two different rhombus channels (a large tubular channel A and small helical channel B) along the c axis (Fig. 2c–e); the diameters of the large channel and the small channel were about $1.3 \times 1.0 \text{ nm}^2$ and $1.1 \times 0.8 \text{ nm}^2$, respectively. Besides the channels along the c axis, the framework also showed large ellipse-like channels along the b axis with the size of about $1.0 \times 1.1 \text{ nm}^2$ (Fig. S3†). Topologically, the framework could be simplified as binodal 4,4-connected topology with the Schläfli symbol of $\{6^4 \cdot 8^2\}\{6^6\}_2$ by assigning the $\text{Cu}_2(\text{CO}_2)_4$ and Cu_4I_4 clusters also as two different 4-connected nodes (Fig. 2f–h). The porous characteristic of the framework further led to the 2-fold interpenetration of two symmetry-related frameworks in the final structure (Fig. 2i). PLATON calculations indicated that the total empty volume of **2** was about 3342.5 \AA^3 , corresponding to 38.6% of the total cell volume (8654 \AA^3). Notably, the void ratio of **2** was much smaller than that of **1**, which may be due to the presence of 2-fold interpenetration in **2**.

Structural description of 3

The SCXRD study revealed that **3** crystallized in the monoclinic $C2/c$ space group. As shown in Fig. S4†, the asymmetric unit holds four Cu^+ ions (Cu1, Cu2, Cu3, Cu4), four Cu^{2+} ions (Cu5, Cu6, Cu7, Cu8), four I^- ions and eight fully deprotonated PVBA $^-$ ligands. The structural SBUs in **3** were similar to those in **1** and **2**. There were two crystallographic unique $\text{Cu}_2(\text{CO}_2)_4$ clusters in **3**. However, the coordination environment was different from those in **1** and **2**. In **3**, the axial position of the $\text{Cu}_2(\text{CO}_2)_4$ clusters was surrounded by two N atoms from two PVBA $^-$ ligands instead of two terminal water ligands in **1** and **2** (Fig. 3a). As a result, each $\text{Cu}_2(\text{CO}_2)_4$ cluster became a 6-connected node to join the neighboring four $\text{Cu}_2(\text{CO}_2)_4$ clusters and two Cu_4I_4 clusters. The Cu_4I_4 cluster served as the same tetrahedral node as those in **1** and **2** (Fig. 3b). One of the interesting structural features in **3** is that the $\text{Cu}_2(\text{CO}_2)_4$ clusters can individually self-assemble into a neutral framework through PVBA $^-$ bridges (Fig. S5a†). The framework possessed rhombic channels along the b axis with the size of $1.5 \times 1.8 \text{ nm}^2$ (Fig. 3c and d). Furthermore, the PVBA $^-$ ligands served as hooks to capture the Cu_4I_4 clusters in half of the rhombic channels (Fig. S5b†). Generally, the self-assembly of PVBA $^-$ with metal ions/clusters would prefer to generate interpenetrated structures since HPVBA is a flexible bridging ligand with a large length.^{36,41} However, due to the

incorporation of the Cu_4I_4 clusters in the channels, the final framework of **3** was a non-interpenetrated structure. Topologically, the $\text{Cu}_2(\text{CO}_2)_4$ clusters could be viewed as 6-connected nodes and the Cu_4I_4 clusters could be viewed as 4-connected nodes. Consequently, **3** displayed 4,6-connected topology with the Schläfli symbol of $\{4^2 \cdot 6^4\}\{4^6 \cdot 6^7 \cdot 8^2\}_2$ (Fig. S6†). PLATON calculations indicated that 56.2% of the total cell volume in **3** belonged to the guest-accessible volume.

Syntheses

During our exploration, we found that some reaction parameters have important impacts on the syntheses of **1–3**. First, the bifunctional ligands HINA and HPVBA are crucial for the assembly of **1–3**. Since the $\text{Cu}_2(\text{CO}_2)_4$ cluster is an O-affinitive SBU and the Cu_4I_4 cluster is a N-affinitive SBU, INA^- and PVBA^- containing both hard carboxylate groups and soft pyridyl groups are quite suitable to bridge these two different SBUs into framework structures according to the hard-soft acid–base theory. Second, the formation of **1–3** is sensitive to organic solvents. When high-boiling solvents (DMA and DEF for **1**, DMA for **2**, and DMF for **3**) were replaced by low-boiling solvents such as CH_3OH , CH_2Cl_2 , CH_3CN , EtOH or H_2O , none of them could be obtained. Third, some non-reactive species also have valuable influence

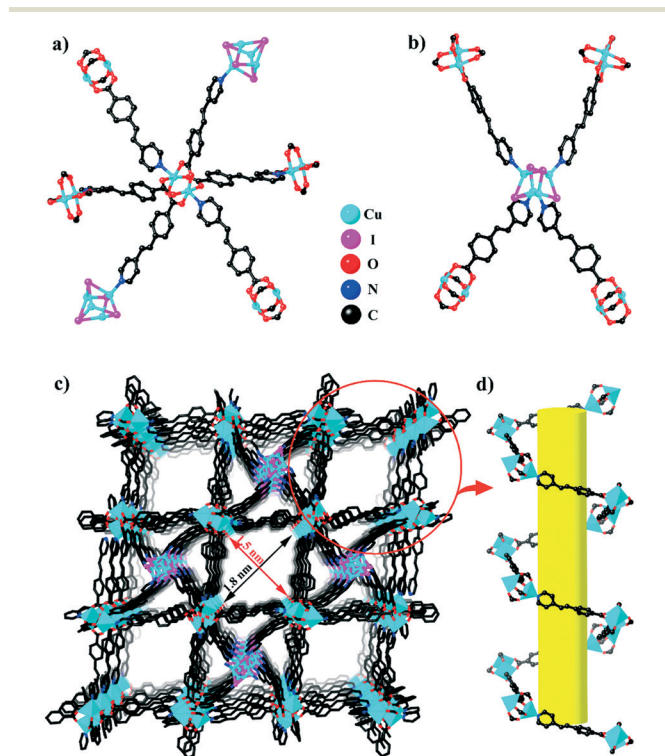


Fig. 3 Crystal structure of **3**: a) view of the coordination environment of the $\text{Cu}_2(\text{CO}_2)_4$ cluster. b) View of the coordination environment of the Cu_4I_4 cluster. c) View of the 3D framework of **3** along the b axis. d) View of the rhombic channels.

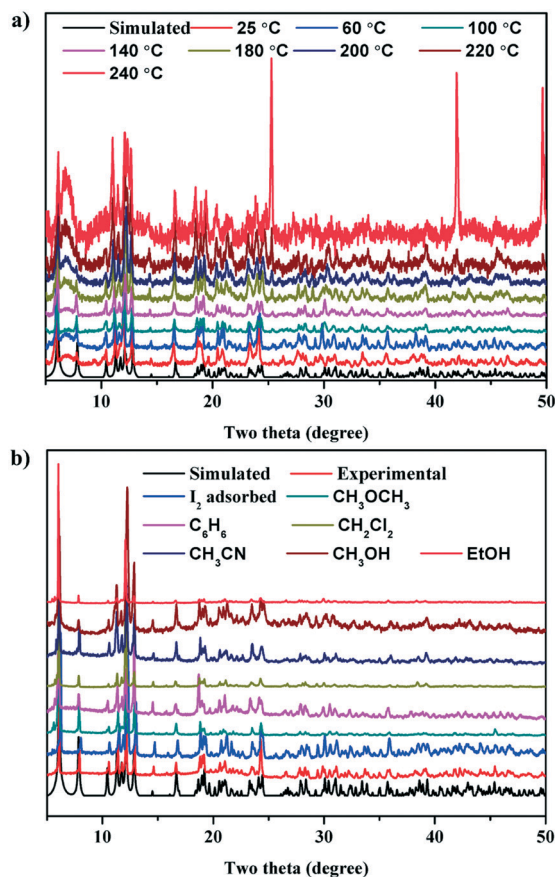


Fig. 4 The PXRD patterns of **2** under a) thermal conditions and b) immersion in a variety of common organic solvents.

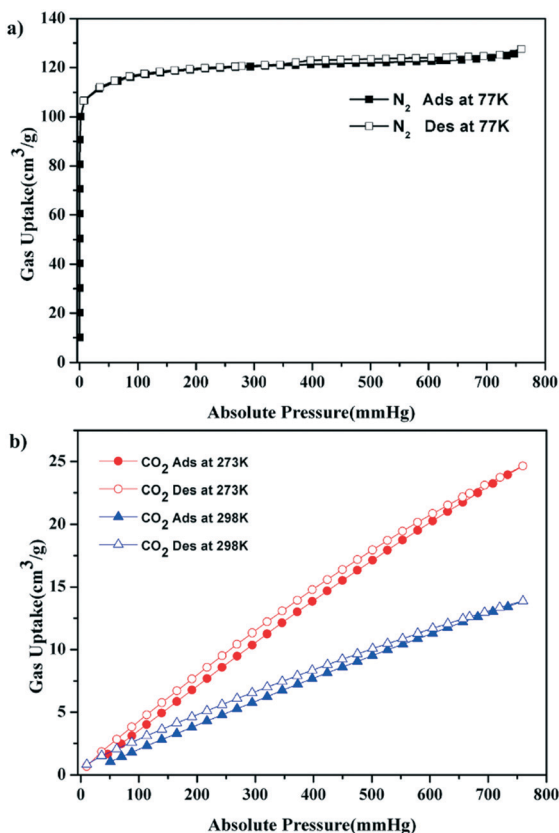


Fig. 5 a) The N_2 and b) CO_2 adsorption isotherms of 2.

on the crystal growth. For example, 4,4'-biphenyldicarboxylic acid is indispensable for the preparation of 1 even though it

is not present in the final structure. 4,4'-Biphenyldicarboxylic acid may have a subtle effect on adjusting the reaction environment to facilitate the formation of 1.

Gas adsorption property

The permanent porosity of the frameworks in 1–3 was initially studied. Unfortunately, the frameworks of 1 and 3 suffered collapse during the activation procedure, which might be ascribed to the high void ratio. Thus, the gas adsorption property of 2 was further studied. Variable-temperature PXRD patterns and solvent stability tests indicated that the framework of 2 was still intact at 240 °C and after being soaked in different low-boiling organic solvents (cyclohexane, CH_2Cl_2 , CH_3CN , CH_3OH , and EtOH) for two days (Fig. 4a and b). As shown in Fig. 5a, the N_2 adsorption of 2 at 77 K displays a reversible type I isotherm typical of a material with permanent microporosity. The calculated saturated uptake and Langmuir/Brunauer–Emmett–Teller (BET) surface areas were $127.56 \text{ cm}^3 \text{ g}^{-1}$ and $530.71/347.23 \text{ m}^2 \text{ g}^{-1}$, which were higher than those of some reported MOFs such as CPM-24 (the Langmuir/BET surface areas are $296/186 \text{ m}^2 \text{ g}^{-1}$).⁴² The corresponding median pore size based on the nonlocal density functional theory was about 8.0 Å (Fig. S10†). Additionally, the CO_2 uptake amounts at 273 and 298 K under 760 mmHg were 24.64 and $13.87 \text{ cm}^3 \text{ g}^{-1}$, respectively (Fig. 5b).

Iodine sorption/release study

The high thermal/solvent stability and the incorporation of cuprous-halide clusters in the framework prompted us to

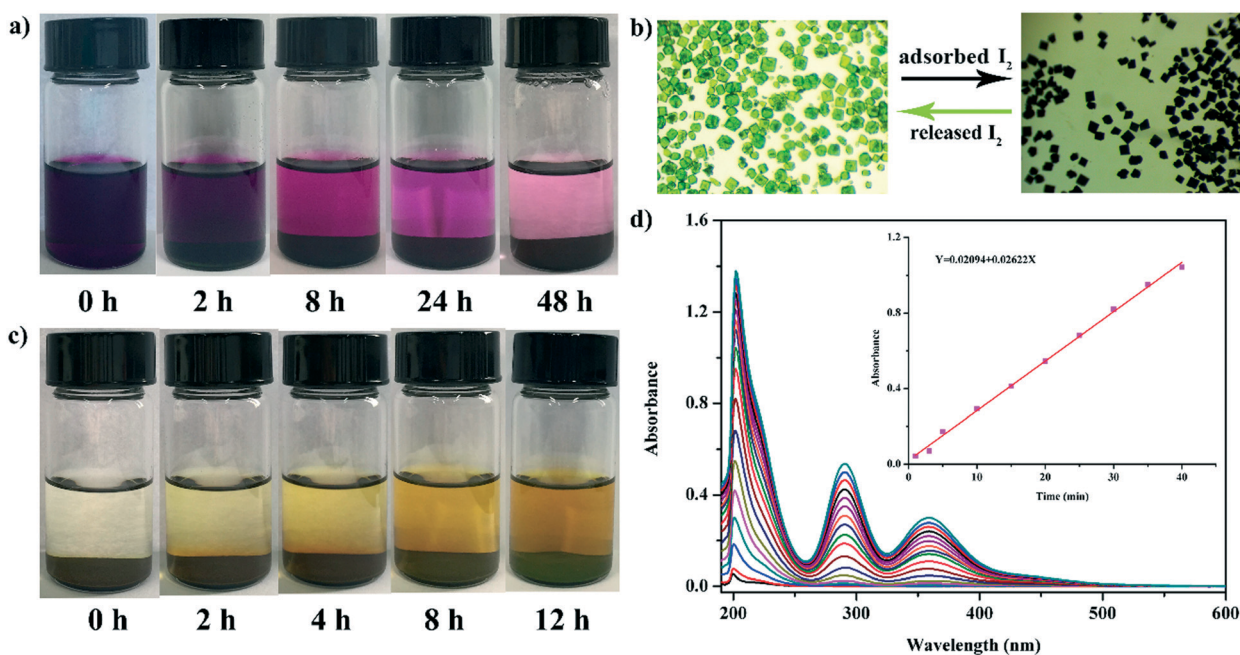


Fig. 6 a) and c) Pictures of different time intervals for the I_2 adsorption/release process in 10 mL of cyclohexane and CH_3OH , respectively. b) Photographs showing the color change of 2 before and after I_2 adsorption. d) I_2 release from $I_2@2$ in CH_3OH at different time intervals. Inset: the release rate of $I_2@2$ in the first 40 min.

evaluate the iodine adsorption and desorption properties of **2**. First, 200 mg of a microcrystalline sample of **2** was immersed in 10 mL of a 0.01 mol L⁻¹ iodine cyclohexane solution in a sealed vial and kept at room temperature. As shown in Fig. 6a, when the crystals of **2** are added to the solution, the colour of the solution gradually changes from dark purple to light pink after 48 hours. Simultaneously, the colour of the crystals changed from light green to black. Interestingly, the shape of the resultant black crystals (denoted as I₂@**2**) showed no obvious change (Fig. 6b). The adsorption capacity of **2** after 48 hours was about 135 mg g⁻¹, which was comparable with that of micro-Cu₄I₄-MOF.⁴³ Also, **2** could adsorb iodine molecules efficiently, which might be attributed to the intermolecular I-I...N and I-I...π halogen bonds.⁴⁴ The PXRD patterns (Fig. 4b) and IR spectra (Fig. S8b†) of I₂@**2** prove that the framework of **2** is still intact after I₂ adsorption. Additionally, the UV-vis spectrum of I₂@**2** displays remarkable adsorption around 530 nm compared with that of **2** (Fig. S11†), which indicates that I₂ molecules enter the framework of **2**. During our study, we also attempted to locate the position of I₂ molecules in I₂@**2** considering that the crystal quality of I₂@**2** is good; however, we failed. In order to further evaluate the I₂ release behaviour of the framework, the crystals of I₂@**2** after the adsorption experiment were immersed in 10 mL CH₃OH. As illustrated in Fig. 6c, the colour of the solution changes from colourless to yellow accompanied with the crystals of I₂@**2** becoming green, indicating that the I₂ molecules in I₂@**2** entered the solution. In order to further investigate the kinetics of iodine desorption, the release process of I₂@**2** was monitored by UV-vis spectroscopy at different intervals based on the intensity variation of the maximum adsorption peak of I₂ (202 nm). As shown in Fig. 6d, the absorbance of I₂@**2** increases linearly over time as a zero-order equation empirically adjusted,⁴⁵ indicating that the release rate of I₂@**2** is relatively stable in the first 40 min. Subsequently, a slow release process was observed, which may be because the concentration of iodine in CH₃OH increased over time (Fig. S12†). By calculations, we found that 0.0875 mg of I₂ was released from I₂-loaded **2** after 120 min according to the standard curve (Fig. S13†). The overall I₂ release content of I₂@**2** was about 75.53%.

Conclusions

In summary, three novel porous cluster organic frameworks **1–3** based on heterovalent paddle-wheel Cu₂(CO₂)₄ and Cu₄I₄ clusters were successfully constructed. The deliberate choice of two bifunctional ligands (HINA and HPVBA) and a linear bridging ligand (DABCO) was crucial for the formation of these new materials. Compounds **1** and **2** possessed 4,4-connected topologies with the Schläfli symbols of {4²-6²-8²}{4²-6⁴} and {6⁴-8²}{6⁶}₂, respectively, while compound **3** exhibited 4,6-connected topology with the Schläfli symbol of {4²-6⁴}{4⁶-6⁷-8²}. Although **1–3** were composed of Cu₂(CO₂)₄ and Cu₄I₄ SBUs, their framework topologies were definitely different,

indicating that Cu₂(CO₂)₄ and Cu₄I₄ are quite flexible SBUs in building framework structures. Furthermore, **2** showed moderate gas uptake ability and I₂ adsorption/release feature. This work not only enriches the limited structural diversities of heterovalent MOF materials, but also provides valuable opinions for the design and fabrication of hybrid materials with intriguing structures and potential applications.

Conflicts of interest

There are no conflicts to declare.

Acknowledgements

This work was financially supported by National Natural Science Foundation of China (No. 21671040 and 21773029).

Notes and references

- 1 A. S. Munn, F. Millange, M. Frigoli, N. Guillou, C. Falaise, V. Stevenson, C. Volkringer, T. Loiseau, G. Cibin and R. I. Walton, *CrystEngComm*, 2016, **18**, 8108.
- 2 X. Zhang, I. D. Silva, H. G. W. Godfrey, S. K. Callear, S. A. Sapchenko, Y. Q. Cheng, I. Vitorica-Yrezabal, M. D. Frogley, G. Cinque, C. C. Tang, C. Giacobbe, C. Dejoie, S. Rudić, A. J. Ramirez-Cuesta, M. A. Denecke, S. Yang and M. Schröder, *J. Am. Chem. Soc.*, 2017, **139**, 16289.
- 3 H. Kitagawa, H. Ohtsu and M. Kawano, *Angew. Chem., Int. Ed.*, 2013, **52**, 12395.
- 4 L. Zhai, Z.-X. Yang, W.-W. Zhang, J.-L. Zuo and X.-M. Ren, *Cryst. Growth Des.*, 2017, **17**, 5263.
- 5 H.-C. Hu, P. Cui, H.-S. Hu, P. Cheng, J. Li and B. Zhao, *Chem. – Eur. J.*, 2018, **24**, 3683.
- 6 Y. H. Xiong, S. S. Chen, F. G. Ye, L. J. Su, C. Zhang, S. F. Shen and S. L. Zhao, *Chem. Commun.*, 2015, **51**, 4635.
- 7 S. Wang, Y. W. Liu, Z. Zhang, X. H. Li, H. R. Tian, T. T. Yan, X. Zhang, S. M. Liu, X. W. Sun, L. Xu, F. Luo and S. X. Liu, *ACS Appl. Mater. Interfaces*, 2019, **11**, 12786.
- 8 G. M. Wang, Z. Z. Xue, J. Pan, L. Wei, S. Han, J. J. Qian and Z. G. Wang, *CrystEngComm*, 2016, **18**, 8362.
- 9 J.-R. Li, D. J. Timmons and H.-C. Zhou, *J. Am. Chem. Soc.*, 2009, **131**, 6368.
- 10 J.-R. Li and H.-C. Zhou, *Nat. Chem.*, 2010, **2**, 893.
- 11 F. Nouar, J. F. Eubank, T. Bousquet, L. Wojtas, M. J. Zaworotko and M. Eddaoudi, *J. Am. Chem. Soc.*, 2008, **130**, 1833.
- 12 N. Zhao, L. Yang, Q. Y. Pan, J. J. Han, X. Li, M. F. Liu, Y. Wang, X. Z. Wang, Q. H. Pan and G. S. Zhu, *Inorg. Chem.*, 2019, **58**, 199.
- 13 X.-X. Li, C.-C. Deng, D. Zhao, H. Yu, Q.-X. Zeng and S.-T. Zheng, *Dalton Trans.*, 2018, **47**, 16408.
- 14 W. Liu, Y. Fang, G. Z. Wei, S. J. Teat, K. Xiong, Z. C. Hu, W. P. Lustig and J. Li, *J. Am. Chem. Soc.*, 2015, **137**, 9400.
- 15 D. Y. Shi, R. Zheng, M.-J. Sun, X. R. Cao, C.-X. Sun, C.-J. Cui, C.-S. Liu, J. W. Zhao and M. Du, *Angew. Chem., Int. Ed.*, 2017, **56**, 14637.
- 16 G. Zeng, S. H. Xing, X. R. Wang, Y. L. Yang, Y. Xiao, Z. H. Li, G. H. Li, Z. Shi and S. H. Feng, *CrystEngComm*, 2016, **18**, 4336.

- 17 J.-H. Liu, Y.-N. Gu, Y. Chen, Y.-J. Qi, X.-X. Li and S.-T. Zheng, *CrystEngComm*, 2018, **20**, 738.
- 18 S. Perruchas, X. F. Le Goff, S. Maron, I. Maurin, F. Guillen, A. Garcia, T. Gacoin and J.-P. Boilot, *J. Am. Chem. Soc.*, 2010, **132**, 10967.
- 19 K. Kirakci, K. Fejfarová, J. Martinčík, M. Nikl and K. Lang, *Inorg. Chem.*, 2017, **56**, 4609.
- 20 Y. Kang, F. Wang, J. Zhang and X. H. Bu, *J. Am. Chem. Soc.*, 2012, **134**, 17881.
- 21 M. S. Deshmukh, A. Yadav, R. Pant and R. Boomishankar, *Inorg. Chem.*, 2015, **54**, 1337.
- 22 M. H. Bi, G. H. Li, J. Hua, Y. L. Liu, X. M. Liu, Y. W. Hu, Z. Shi and S. H. Feng, *Cryst. Growth Des.*, 2007, **7**, 2066.
- 23 X.-X. Li, X. Ma, W.-X. Zheng, Y.-J. Qi, S.-T. Zheng and G.-Y. Yang, *Inorg. Chem.*, 2007, **55**, 8257.
- 24 X. L. Luo, L. B. Sun, J. Zhao, D.-S. Li, D. M. Wang, G. H. Li, Q. S. Huo and Y. L. Liu, *Cryst. Growth Des.*, 2015, **15**, 4901.
- 25 (a) R. J. Huang and T. Hoffmann, *Anal. Chem.*, 2009, **81**, 1777; (b) L. J. Carpenter, *Chem. Rev.*, 2003, **103**, 4953.
- 26 C. Hayakawa, K. Urita, T. Ohba, H. Kanoh and K. Kaneko, *Langmuir*, 2009, **25**, 1795.
- 27 D. F. Sava, M. A. Rodriguez, K. W. Chapman, P. J. Chupas, J. A. Greathouse, P. S. Crozier and T. M. Nenoff, *J. Am. Chem. Soc.*, 2011, **133**, 12398.
- 28 M.-H. Zeng, Q.-X. Wang, Y.-X. Tan, S. Hu, H.-X. Zhao, L.-S. Long and M. Kurmoo, *J. Am. Chem. Soc.*, 2017, **132**, 2561.
- 29 D. F. Sava, K. W. Chapman, M. A. Rodriguez, J. A. Greathouse, P. S. Crozier, H. Zhao, P. J. Chupas and T. M. Nenoff, *Chem. Mater.*, 2013, **25**, 2591.
- 30 H.-X. Zhang, X. D. Yan, Y.-X. Chen, S.-H. Zhang, T. Li, W.-K. Han, L.-Y. Bao, R. Shen and Z.-G. Gu, *Chem. Commun.*, 2019, **55**, 1120.
- 31 E. Baladi, V. Nobakht, A. Tarassoli, D. M. Proserpio and L. Carlucci, *Cryst. Growth Des.*, 2018, **18**, 7207.
- 32 M. W. Jia, J. T. Li, S. T. Che, L. Kan, G. H. Lia and Y. L. Liu, *Inorg. Chem. Front.*, 2019, **6**, 1261.
- 33 J. Wang, J. H. Luo, X. L. Luo, J. Zhao, D.-S. Li, G. H. Li, Q. S. Huo and Y. L. Liu, *Cryst. Growth Des.*, 2015, **15**, 915.
- 34 S. Yao, X. D. Sun, B. Liu, R. Krishna, G. H. Li, Q. S. Huo and Y. L. Liu, *J. Mater. Chem. A*, 2016, **4**, 15081.
- 35 J. Q. Yuan, J. T. Li, L. Kan, L. F. Zou, J. Zhao, D.-S. Li, G. H. Li, L. Zhang and Y. L. Liu, *Cryst. Growth Des.*, 2018, **18**, 5449.
- 36 S. K. Elsaidi, M. H. Mohamed, L. Wojtas, A. Chanthapally, T. Pham, B. Space, J. J. Vittal and M. J. Zaworotko, *J. Am. Chem. Soc.*, 2014, **136**, 5072.
- 37 G. M. Sheldrick, *Acta Crystallogr., Sect. A: Found. Crystallogr.*, 2008, **64**, 112.
- 38 (a) A. L. J. Spek, *Acta Crystallogr., Sect. A: Found. Crystallogr.*, 2003, **36**, 7; (b) P. V. D. Sluis and A. L. Spek, *Acta Crystallogr., Sect. A: Found. Crystallogr.*, 1990, **46**, 194.
- 39 Z.-Z. Xue, D. Zhang, J. Pan, S.-D. Han, J.-H. Li and G.-M. Wang, *Dalton Trans.*, 2017, **46**, 13952.
- 40 (a) J. J. Qian, F. L. Jiang, K. Z. Su, J. Pan, Z. Z. Xue, L. F. Liang, P. P. Bag and M. C. Hong, *Chem. Commun.*, 2014, **50**, 15224; (b) T. Granca, J. Ferrando-Soria, D. M. Proserpio and D. Armentano, *Inorg. Chem.*, 2018, **57**, 12869; (c) L. Martins, L. K. Macreadie, D. Sensharma, S. Vaesen, X. Zhang, J. J. Gough, M. ÓDoherty, N.-Y. Zhu, M. Rüther, J. E. ÓBrien, A. Louise Bradley and W. Schmitt, *Chem. Commun.*, 2019, **55**, 5013; (d) H. Hu, J. X. Zhu, F. L. Yang, Z. X. Chen, M. L. Deng, L. H. Weng, Y. Ling and Y. Zhou, *Chem. Commun.*, 2019, **55**, 6495.
- 41 M. K. Sharma, P. Lama and P. K. Bharadwaj, *Cryst. Growth Des.*, 2011, **11**, 1411.
- 42 S.-T. Zheng, T. Wu, B. Irfanoglu, F. Zuo, P. Y. Feng and X. H. Bu, *Angew. Chem.*, 2011, **123**, 8184.
- 43 N.-X. Zhu, C.-W. Zhao, J.-C. Wang, Y.-A. Li and Y.-B. Dong, *Chem. Commun.*, 2016, **52**, 12702.
- 44 R.-X. Yao, X. Cui, X.-X. Jia, F.-Q. Zhang and X.-M. Zhang, *Inorg. Chem.*, 2016, **55**, 9270.
- 45 Z. Yin, Q.-X. Wang and M.-H. Zeng, *J. Am. Chem. Soc.*, 2012, **134**, 4857.